BJRS
BRAZILIAN JOURNAL OF RADIATION SCIENCES

doi.org/10.15392/2319-0612.2024.2556
2024, 12(4) | 01-24 | e2556
Submitted: 2024-07-12
Accepted: 2024-09-17

Material imaging study of 3D printing materials for diagnostic radiology phantom development

Oliveira[a*], M. V. L.; Savi [b], M.; Vitor[b], A.; Villani[c,d], D.; Andrade[b,f], M. A.B.; Ubeda[f], C.; Mitsuo[a], M.M.

[a] Federeal Institute of Education, Science, Technology of Bahia, 40301-015, Salvador, Bahia, Brasil.
[b] Department of Health. Federal Institute of Education, Science and Technology of Santa Catarina –IFSC, 88020-300, Florianópolis, Santa Catarina (SC), Brazil

[c] Instituto de Pesquisas Energéticas e Nucleares – IPEN/USP, 05508-000, São Paulo, São Paulo, Brazil

[d] Photo Injector Test Facility – PITZ, Deutsches Elektronen-Synchrotron-DESY. ,Platanenallee 6, 15738 Zeuthen, Germany

[e] Federal University of Santa Catarina,88036-800, Florianopolis, Santa Catarina, Brazil

[f] Medical Technology Department. Health Sciences Faculty, Tarapaca University, 1010069, Arica, Chile.

*Correspondence: marcusradiology@gmail.com

Abstract: The 3D printing techniques have found applications across diverse fields, significantly enhancing design and manufacturing processes. The impact of this growth is particularly notable in radiology, where 3D printing has been applied to developing quality control tools and advancing dosimetry techniques. 3D printing has the advantage of having a wide variety of plastic materials which can be used in the manufacturing process; there is a scarcity of work developed to evaluate the attenuation of the x-ray beam of the materials used in printing 3D models for phantom development. This paper aims to show our results on the imaging characteristics investigation of 15 3D printable materials. 3D objects were printed as cubes of 20 x 20 x 20 mm3 with a 100% infill and 45°/45° rectilinear structural pattern, and images acquired in a DR X-ray unit were analyzed with ImageJ software. Imaging pixel values, Signal-to-Noise Ratio – signal-to-noise ratio and Contrast-to-Noise Ratio – contrast-to-noise ratio were evaluated and compared between the 3D-printed cubes and a standard chest phantom. When comparing the SIGNAL-TO-NOISE RATIO for plastic materials and chest structures, significant differences were found. Similar results were found for the contrast-to-noise ratio. The differences were noted by the use of Kruskal Wallis test for both plastic materials, Tungsten and Bismuth, that demonstrated statistically significant values of signal-to-noise ratio compared to the lung ($p < 0.0001$) and right rib ($p < 0.0001$). Tungsten and Bismuth filaments were found to have the potential to represent the signal-to-noise ratio for intermediary and high-density structures. Scapula was the only anatomical structure with no statistically significant difference of the contrast-to-noise ratio for SILK ($p \geq 0.074$), ABS ($p \geq 0.086$), PVA ($p \geq 0.917$) and ABSpremium ($p \geq 0.955$). The study of potential radiological 3D printing materials for diagnostic radiology phantom development revealed important imaging characteristics for the plastic materials using the Fused Filament Fabrication technique.

SBPR

BJRS
BRAZILIAN JOURNAL OF RADIATION SCIENCES

doi.org/10.15392/2319-0612.2024.2556
2024, 12(4) | 01-24 | e2556
Submitted: 2024-07-12
Accepted: 2024-09-17

Keywords: 3D printing, phantom, Fused Filament Fabrication, Signal-to-Noise Ratio, Contrast-to-Noise Ratio.

SBPR

BJRS
BRAZILIAN JOURNAL OF RADIATION SCIENCES

doi.org/10.15392/2319-0612.2024.2556
2024, 12(4) | 01-24 | e2556
Submitted: 2024-07-12
Accepted: 2024-09-17

Estudo da imagem de materiais impressos em 3D para desenvolvimento de fantomas para radiologia diagnóstica

Resumo: As técnicas de impressão 3D têm encontrado aplicações em diversos campos, melhorando significativamente os processos de design e fabricação. O impacto deste crescimento é perceptível na radiologia, onde a impressão 3D tem sido aplicada ao desenvolvimento de ferramentas de controle de qualidade e ao avanço de técnicas de dosimetria. A impressão 3D tem a vantagem de possuir uma grande variedade de materiais plásticos que podem ser utilizados no processo de fabricação. Há escassez de trabalhos desenvolvidos para avaliar a atenuação do feixe de raios X dos materiais utilizados na impressão de modelos 3D para desenvlvimento de fantomas. Este artigo tem como objetivo mostrar nossos resultados na pesquisa das características de imagem de 15 materiais impressos em 3D. Os objetos 3D foram impressos como cubos de 20 x 20 x 20 mm^3 com preenchimento de 100%, padrão estrutural retilíneo de 45°/45°. As imagens foram adquiridas em uma unidade de raios X DR e foram analisadas com o software ImageJ. Os valores dos pixels de imagem, a relação sinal-ruído – SNR e a relação contraste-ruído – CNR foram avaliados e comparados entre os cubos impressos em 3D e um simulador de tórax padrão. Ao comparar a relação sinal-ruído para materiais plásticos e estruturas torácicas, foram encontradas diferenças significativas. Resultados semelhantes foram encontrados para o relação contraste-ruído. As diferenças foram notadas por meio do teste de Kruskal Wallis para os materiais plásticos Tungstênio e Bismuto que demonstraram valores estatisticamente significativos de relação sinal-ruído signal-to-noise ratio em comparação ao pulmão ($p < 0,0001$) e à costela direita ($p < 0,0001$). descobriu-se que os filamentos de tungstênio e bismuto têm potencial para representar o relação sinal-ruído para estruturas intermediárias e de alta densidade. a escápula foi a única estrutura anatômica sem diferença estatisticamente significativa do relação contraste-ruído em realação ao SILK ($p \geq 0,074$), ABS ($p \geq 0,086$), PVA ($p \geq 0,917$) e ABSpremium ($p \geq 0,955$). O estudo demonstrou potenciais materiais de impressão 3D para desenvolvimento de simuladores de radiologia diagnóstica e revelou importantes características de imagem para os materiais plásticos usando a técnica Fused Filament Fabrication.

Palavras-chave: Impressão 3D, fantoma, radiologia diagnóstica.

SBPR

1. INTRODUCTION

The technique of 3D printing, which has significantly evolved over the past few decades[1], has revolutionized how to create and visualize three-dimensional objects. This innovative technology, facilitated by advanced computer systems, has found applications across diverse fields, significantly enhancing design and manufacturing processes. The impact of this growth is particularly notable in radiology, where 3D printing has been instrumental in developing quality control tools and advancing dosimetry techniques [2]. The vast array of available technologies further underscores the versatility of 3D printing. Fused Filament Fabrication (FFF), also known as Fused Deposition Modeling (FDM), stands out as the most prevalent [3]. The thermoplastic filaments are made up of different types of polymers and varied formulations, and the most common materials are made of Acrylonitrile Butadiene Styrene (ABS), which is derived from petroleum, and Polylactic Acid (PLA)[4,5].

The extensive growth of 3D printing has led to the creation of 3D objects for use in transplants, pediatrics and surgery. This ongoing evolution of 3D printing techniques continues to unlock new possibilities for future advancements in various sectors [6]. In addition, 3D printing has fostered many research opportunities for tool developments using computed tomography technology to identify correspondent material with similar attenuation proprieties to human tissue. In previous work, Savi and collaborators [7] tested 17 different materials varying infill type and percentage to characterize which material presents the best tissue concordance. Also, they developed radiopaque filaments made from a blend of ABS, Barium Sulfate and Calcium Carbonate to mimic cortical bone, enamel and dentin [8]. Both studies confirm that the relation between Hounsfield units and infill percentage is linear.

Few studies still report the development of 3D objects for quality control in the context of X-ray equipment [9–12] . Furthermore, radiology facilities demand the use of phantoms for

image quality evaluation, and usually, these phantoms are considered too expensive and delicate to handle [13–15]. 3D printing has demonstrated potential for phantom construction of the breast [16–18], the whole body [19], the head [20], and the spine [21].

Although 3D printing has the advantage of having a wide variety of plastic materials which can be used in the manufacturing process, there needs to be more work developed to evaluate the attenuation of the x-ray beam of the materials used in printing 3D models for phantom development. Recently, a paper concluded a notable gap in the representation of essential thoracic structures for comprehensive chest phantom development[22]. This paper aims to show our results on the imaging characteristics investigation of fifteen 3D printable materials, in order to respond the following question: which and how the evaluated 3D printing materials can be used as material do develop 3D printing phantoms when evaluated in digital radiography?

2. MATERIALS AND METHODS

2.1. 3D printing materials

In this study, a GTMax Core H4 printer was used. 3D objects were printed as cubes with dimensions 20 x 20 x 20 mm^3 (Figure 1). All cubes were placed on the Polymethyl Methacrylate (PMMA) holder with 20 cm thickness. In total, fifteen 3D filaments were evaluated: 1) PETG (Polyethylene Terephthalate Glycol), 2) Aluminum, 3) ABS premium (Acrylonitrile Butadiene Styrene), 4) Copper, 5) PVA (Polyvinyl Alcohol), 6) TPE (Thermoplastic elastomer), 7) PLA-SILK, 8) TPU (thermoplastic polyurethane), 9) Bronze, 10) WOOD, 11) BONE, 12) ABS (Acrylonitrile Butadiene Styrene), 13) PLA (Polylactic Acid), 14) Tungsten, and 15) Bismuth.

The filaments were grouped into three classes as follows:

- Three composed the ABS based materials being regular ABS, ABS premium and ABS with wood dust;
- Six PLA-based filaments. Besides regular PLA and one named SILK, the other four have different fillers mixed in the matrix like Aluminum, Copper and one made with 2% cow bone and
- The last five are groped in "other plastic bases", such as HIPS, PETG, PVA, TPU, and TPE.

2.2. Imaging protocols

In total, nine different imaging protocols (tube potentials of 60 kV, 70kV, 80kV, and time-current product 2.5mAs, 5mAs, and 10mAs) were used to obtain the images in a DR X-ray unit (Konica Minolta, Altus DR). The same protocols were applied to obtain the images of an adult anthropomorphic phantom of the chest (Radiation Support Devices, model RS-111) with anteroposterior acquisition. The focal spot-detector distance was set to 100 cm. In the study, we exclusively evaluated cubes that featured a 100% infill and 45°/45° rectilinear structural pattern for our evaluation. This selection was made to mitigate the influence of bubbles or air gaps between the layers of deposited plastic material inherent from the FFF 3D printing technique.

2.3. Imaging data analysis

The digital images were evaluated using ImageJ software [23] (Version 1.53, US National Institutes of Health and the Laboratory for Optical and Computational Instrumentation (LOCI, University of Wisconsin)), USA, using Contrast-to-Noise Ratio and Signal-to-Noise Ratio measurement [24].

The DICOM image acquired was uploaded to the ImageJ [23] software and analyzed using a plugin to standard the region of interest (ROI) size and save the results of measurements

(mean, standard deviation, Signal-to-Noise Ratio – signal-to-noise ratio and Contrast-to-Noise Ratio – CNR) automatically as an Excel spreadsheet. The standard ROI size (with 100 pixels included) was used to evaluate all the materials and radiographic landmarks. In terms of radiographic image, in total, seven ROIs were placed on: 1) the sixtieth rib, 2) the fiftieth vertebra, 3) the heart, 4) the apex of the lung, 5) the scapula, 6) soft tissue, 7) liver.

Regarding contrast-to-noise ratio, the mean greyscale values ($Signal_{Material}$) and the standard deviation of the greyscale values (SD_{BG}) were obtained using the plugin. Three experienced professionals performed the measurements, placing the ROI in the surrounding background and in the structures. Both parameters were used to find the contrast-to-noise ratio using of equation 1. For the cube setup, the PMMA slab was considered the background to the cubes set up, whereas, for the chest phantom, the soft tissue was considered the background ($Signal_{Bg}$) for chest set up. The ROI was placed on the right lateral region of the chest phantom, next to the scapula, for soft tissue.

$$CNR = \frac{Signal_{material} - Signal_{Bg}}{SD_{Bg}} \quad \text{Eq. (1)}$$

The Signal-to-Noise Ratio was calculated using the equation 2, where $Signal_{material}$ corresponds to the mean grey value within the ROI and the $SD_{Material}$ is the standard deviation of the mean grey values in the ROI.

$$SNR = \frac{Signal_{material}}{SD_{Material}} \quad \text{Eq. (2)}$$

The data were imported to Statistical Package for the Social Sciences, SPSS (version 28, 2021) for analysis. The non-parametric Kruskal Wallis test was carried out to evaluate the statistical significance of signal-to-noise ratio and contrast-to-noise ratio values of the plastic materials' and chest phantom structures' signal-to-noise ratio and contrast-to-noise ratio values. The p-value > 0.05 was considered to have no statistical significance. These statistical evaluations aimed to show the agreement between phantom structures and 3D printing material attenuation and imaging value.

Figure 1. Set up of experiment: a) 3D-printed cubes of materials on the PMMA slab, b) Adult anthropomorphic phantom of the chest with anteroposterior acquisition.

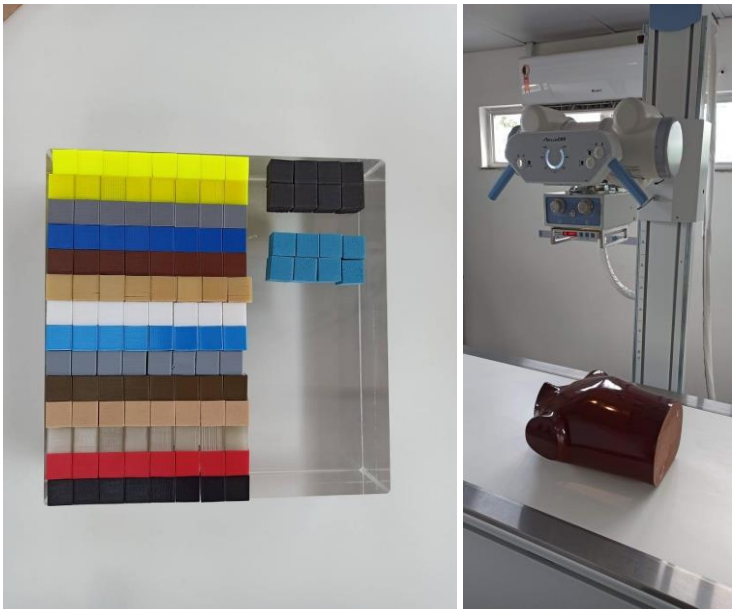

3. RESULTS AND DISCUSSIONS

Figure 2 show the radiographic images from the cubes and the anthropomorphic phantom with the ROIs for evaluation.

Figure 2. X-ray image of the a) the chest anthropomorphic phantom with regions of interest (ROI) placed on the anatomical landmarks and b) the 3D-printed plastic materials.

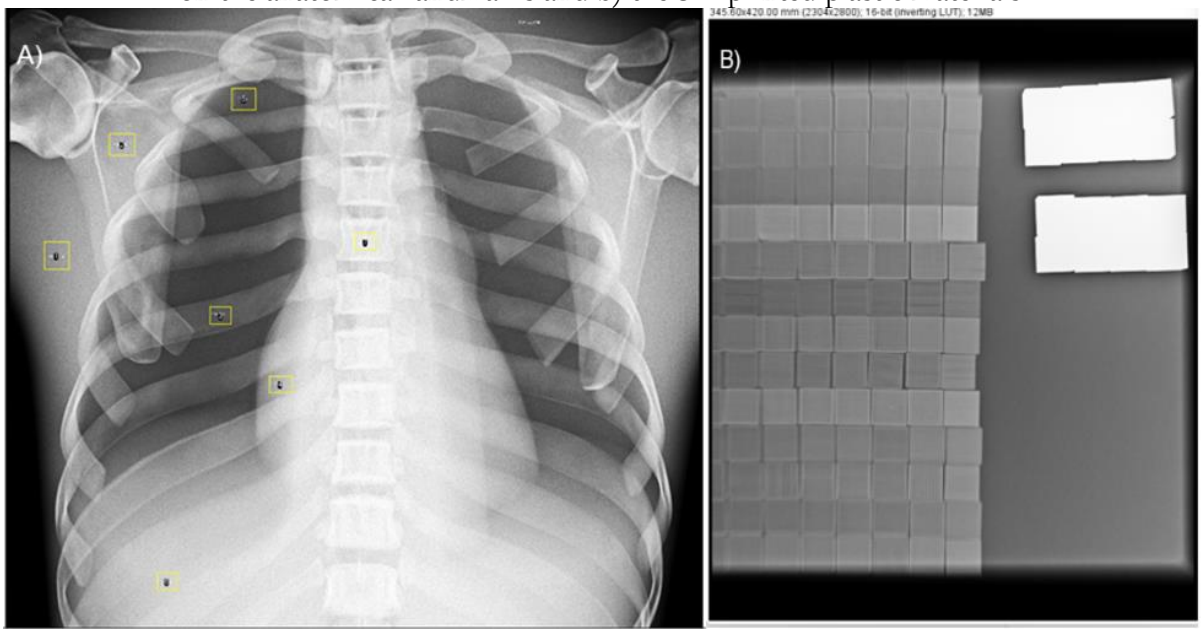

Figures 3 and 4 show the mean pixel value for plastic materials and anthropomorphic phantom, according to imaging protocol used.

Figure 3. Plastic material Mean pixel value for imaging protocol used.

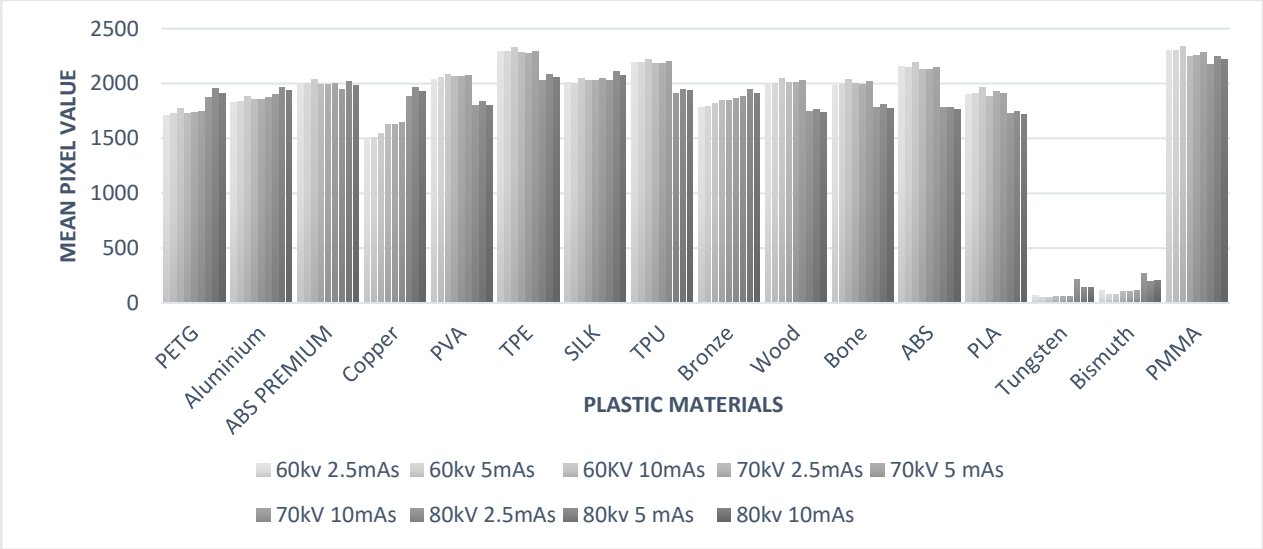

Figure 4. Anthropologic phantom Mean pixel value for diverse protocols

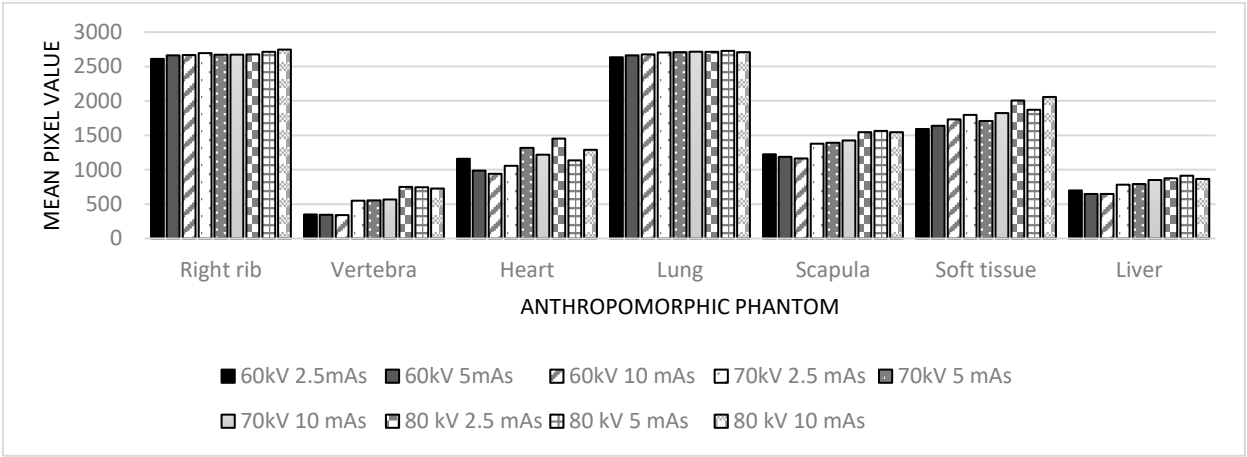

The noise level for both plastic materials and anthropomorphic phantom are shown in Figures 5 and 6. For both objects (cube and phantom), the materials/structures with higher attenuation showed lower noise level.

Figure 5. Noise level on the plastic materials imaging for imaging protocol used

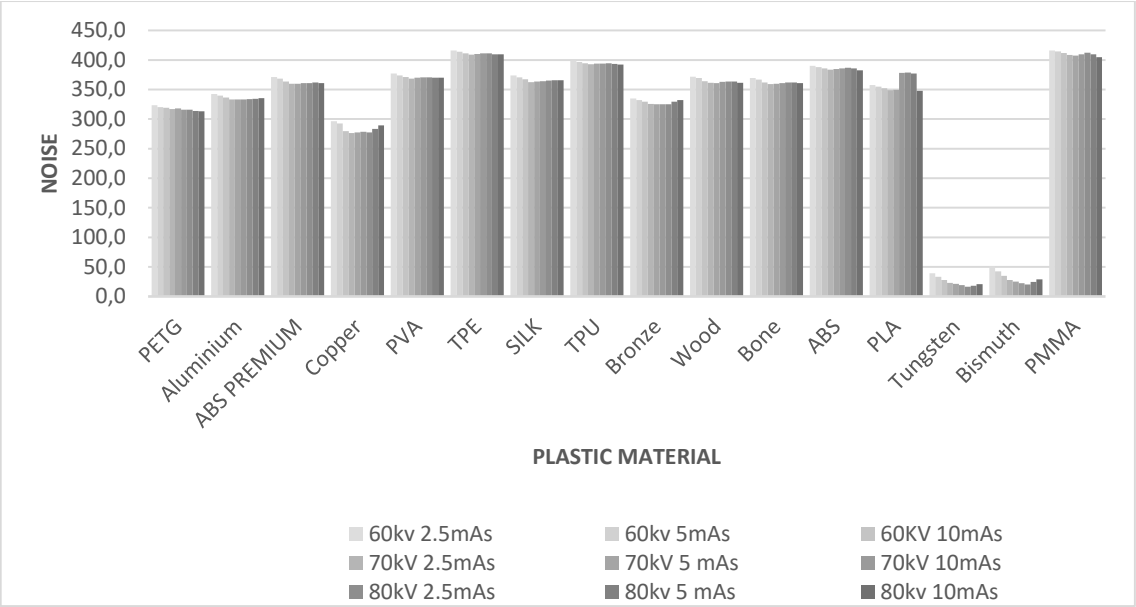

Figure 6. Noise level on the anthropomorphic phantom imaging for imaging protocol used

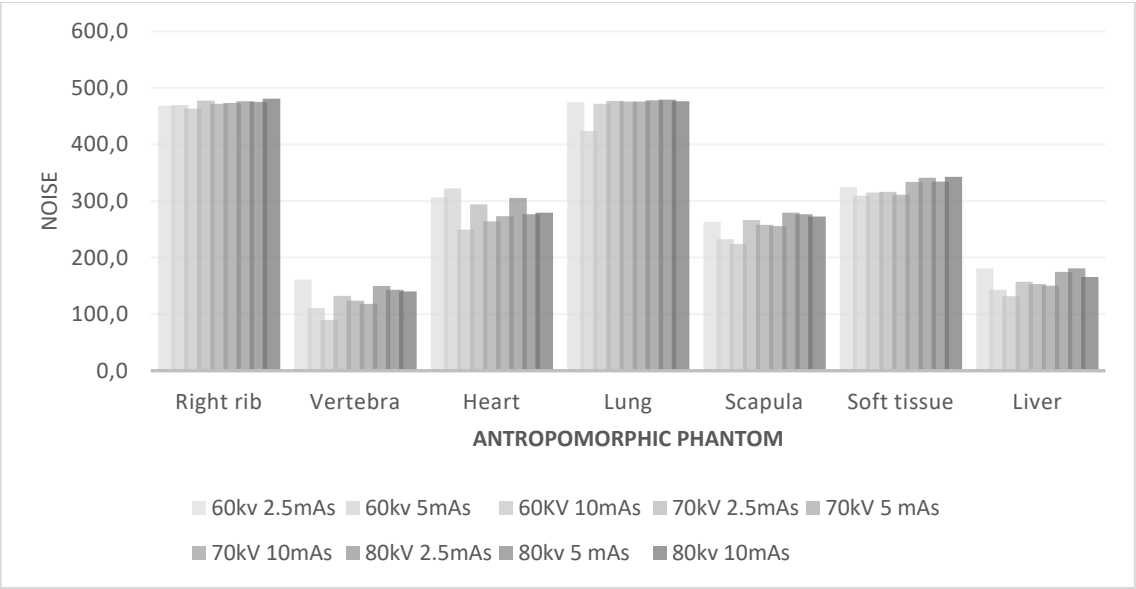

The distribution of the contrast-to-noise ratio of the structures, filtered by protocols, concerning plastic materials and anthropomorphic phantom was evaluated. In this analysis, the PMMA holder (cube setup) and the soft tissue of the phantom were regarded as background.

Table 1. Signal-to-Noise Ratio (SNR) and Contrast- to Noise Ratio (CNR) of the 3D-printed plastic materials and anthropomorphic phantom structures

	Plastic materials			Anthropomorphic Phantom		
	Label	**SNR**	**CNR**	**Label**	**SNR**	**CNR**
60kV 2.5 mAs	PETG	5.31	1.42	Right rib	5.58	3.11
	Aluminium	5.35	1.13	Vertebra	2.13	3.80
	ABS PREMIUM	5.41	0.74	Heart	3.80	1.32
	Copper	5.20	1.95	Lung	5.52	3.18
	PVA	5.40	0.64	Scapula	4.48	1.13
	TPE	5.49	0.03	Soft tissue	4.87	
	SILK	5.38	0.70	Liver	3.85	2.74
	TPU	5.45	0.27			
	Bronze	5.30	1.25			
	Wood	5.38	0.72			
	Bone	5.40	0.77			
	ABS	5.51	0.36			
	PLA	5.32	0.97			
	Tungsten	1.60	5.37			
	Bismuth	2.07	5.26			
	PMMA	5.53				
60kV 5 mAs	PETG	5.51	1.44	Right rib	5.65	3.26
	Aluminium	5.52	1.15	Vertebra	3.04	4.12
	ABS premium	5.57	0.75	Heart	3.86	2.07
	Copper	5.45	1.99	Lung	5.63	3.26
	PVA	5.57	0.64	Scapula	5.10	1.43
	TPE	5.61	0.04	Soft tissue	5.22	
	SILK	5.52	0.73	Liver	4.68	3.16
	TPU	5.58	0.29			
	Bronze	5.48	1.25			
	WOOD	5.55	0.70			
	BONE	5.55	0.78			
	ABS	5.61	0.40			
	PLA	5.52	0.93			
	TUNGS	2.48	5.47			
	BISMUTH	2.61	5.45			
	PMMA	5.62				

	Plastic materials			Anthropomorphic Phantom		
	Label	**SNR**	**CNR**	**Label**	**SNR**	**CNR**
60kV 10 mAs	PETG	5.61	1.35	Right rib	5.68	2.92
	Aluminium	5.62	1.08	Vertebra	3.77	4.34
	ABS premium	5.64	0.70	Heart	4.22	2.46
	Copper	5.56	1.88	Lung	5.65	2.95
	PVA	5.62	0.55	Scapula	5.20	1.77
	TPE	5.65	-0.05	Soft tissue	5.40	
	SILK	5.60	0.64	Liver	5.18	3.38
	TPU	5.64	0.20			
	Bronze	5.58	1.21			
	WOOD	5.62	0.66			
	BONE	5.62	0.70			
	ABS	5.65	0.31			
	PLA	5.58	0.88			
	TUNGS	3.25	5.51			
	BISMUTH	3.65	5.50			
	PMMA	5.67				
70kV 2.5 mAs	PETG	5.52	1.35	Right rib	5.65	2.69
	Aluminium	5.54	0.99	Vertebra	3.88	3.72
	ABS premium	5.53	0.60	Heart	4.34	2.20
	Copper	5.48	1.57	Lung	5.65	2.72
	PVA	5.56	0.47	Scapula	5.18	1.25
	TPE	5.61	-0.11	Soft tissue	5.37	
	SILK	5.53	0.51	Liver	5.00	3.04
	TPU	5.58	0.13			
	Bronze	5.50	0.94			
	WOOD	5.57	0.56			
	BONE	5.55	0.61			
	ABS	5.60	0.26			
	PLA	5.40	0.94			
	TUNGS	2.80	5.45			
	BISMUTH	3.00	5.39			
	PMMA	5.63				

	Plastic materials			Anthropomorphic Phantom		
	Label	**SNR**	**CNR**	**Label**	**SNR**	**CNR**
70kV 5 mAs	PETG	5.61	1.33	Right rib	5.68	3.08
	Aluminium	5.61	1.01	Vertebra	4.36	3.69
	ABS premium	5.63	0.63	Heart	4.54	1.25
	Copper	5.58	1.60	Lung	5.67	3.20
	PVA	5.63	0.47	Scapula	5.39	1.01
	TPE	5.66	-0.06	Soft tissue	5.46	
	SILK	5.62	0.56	Liver	5.39	2.93
	TPU	5.64	0.17			
	Bronze	5.60	0.99			
	WOOD	5.63	0.63			
	BONE	5.62	0.66			
	ABS	5.65	0.33			
	PLA	5.60	0.80			
	TUNGS	3.72	5.50			
	BISMUTH	4.08	5.42			
	PMMA	5.67				
70kV 10 mAs	PETG	5.65	1.36	Right rib	5.70	2.57
	Aluminium	5.66	1.04	Vertebra	4.36	3.81
	ABS premium	5.68	0.72	Heart	4.68	1.83
	Copper	5.63	1.65	Lung	5.69	2.70
	PVA	5.67	0.54	Scapula	5.50	1.21
	TPE	5.67	-0.01	Soft tissue	5.52	
	SILK	5.65	0.59	Liver	5.56	2.95
	TPU	5.66	0.21			
	Bronze	5.65	1.06			
	WOOD	5.66	0.66			
	BONE	5.64	0.66			
	ABS	5.67	0.33			
	PLA	5.62	0.86			
	TUNGS	4.50	5.50			
	BISMUTH	4.62	5.44			
	PMMA	5.68				

	Plastic materials			Anthropomorphic Phantom		
	Label	**SNR**	**CNR**	**Label**	**SNR**	**CNR**
80kV 2.5 mAs	PETG	5.66	0.65	Right rib	5.69	1.84
	Aluminium	5.65	0.61	Vertebra	4.70	3.47
	ABS premium	5.66	0.50	Heart	4.69	1.52
	Copper	5.62	1.20	Lung	5.67	1.95
	PVA	5.64	0.62	Scapula	5.49	1.27
	TPE	5.63	0.21	Soft tissue	5.53	
	SILK	5.64	0.88	Liver	5.34	3.12
	TPU	5.66	0.74			
	Bronze	5.63	1.33			
	WOOD	5.64	1.13			
	BONE	5.64	1.29			
	ABS	5.66	1.29			
	PLA	4.99	4.82			
	TUNGS	5.14	4.74			
	BISMUTH	5.68	0.08			
	PMMA	5.68				
80kV 5 mAs	PETG	5.67	0.62	Right rib	5.69	2.50
	Aluminium	5.67	0.52	Vertebra	5.14	3.34
	ABS premium	5.68	0.41	Heart	4.67	2.18
	Copper	5.63	1.25	Lung	5.69	2.55
	PVA	5.65	0.53	Scapula	5.57	0.91
	TPE	5.63	0.06	Soft tissue	5.55	
	SILK	5.64	0.90	Liver	5.55	2.85
	TPU	5.66	0.70			
	Bronze	5.64	1.39			
	WOOD	5.65	1.18			
	BONE	5.62	1.35			
	ABS	5.66	1.32			
	PLA	5.05	5.19			
	TUNGS	5.05	5.15			
	BISMUTH	5.69	0.23			
	PMMA	5.69				

	Plastic materials			Anthropomorphic Phantom		
	Label	**SNR**	**CNR**	**Label**	**SNR**	**CNR**
80kV 10 mAs	PETG	5.68	0.65	Right rib	5.70	1.87
	Aluminium	5.68	0.58	Vertebra	5.35	3.63
	ABS premium	5.68	0.45	Heart	4.90	2.10
	Copper	5.66	1.30	Lung	5.67	1.77
	PVA	5.67	0.52	Scapula	5.55	1.40
	TPE	5.64	0.09	Soft tissue	5.61	
	SILK	5.67	0.89	Liver	5.49	3.25
	TPU	5.67	0.76			
	Bronze	5.68	1.46			
	WOOD	5.67	1.25			
	BONE	5.64	1.39			
	ABS	5.66	1.35			
	PLA	5.22	5.21			
	TUNGS	5.27	5.16			
	BISMUTH	5.71	0.21			
	PMMA	5.70				

The independent sample Kruskal – Wallis test showed that the distribution of Signal-to-Noise Ratio was statistically significant ($p < 0.001$). The pairwise comparison shows which cases had significant differences in signal-to-noise ratio (Table 2). Table 3 shows the comparison between the contrast-to-noise ratio values.

Table 2. Pairwise-comparison of Signal-to-Noise Ratio (SNR) between 3D-printed plastic materials and anthropomorphic phantom structures

Plastic material	Anthropomorphic Phantom	Significance
Tungsten	Vertebra	1.000
	Heart	1.000
	Liver	1.000
	Scapula	1.000
	Soft Tissue	0.341
	Lung	<0.001
	Right Rib	<0.001
Bismuth	Vertebra	1.000
	Heart	1.000
	Liver	1.000
	Scapula	1.000
	Soft Tissue	0.677
	Lung	<0.001
	Right Rib	<0.001

p-value of < 0.05 was considered as statistically significant

Table 3. Pairwise-comparison of Contrast-to-Noise Ratio (CNR) between 3D-printed plastic materials and anthropomorphic phantom structures

Plastic material	Anthropomorphic Phantom	Significance
TPE	Scapula	<0.001
	HEART	<0.001
	LUNG	<0.001
	LIVER	<0.001
	Right Rib	<0.001
	Vertebra	<0.001
TPU	Scapula	0.002
	HEART	<0.001
	LUNG	<0.001
	LIVER	<0.001
	Right Rib	<0.001
	Vertebra	<0.001
SILK	Scapula	0.074
	HEART	<0.001
	LUNG	<0.001
	LIVER	<0.001
	Right Rib	<0.001
	Vertebra	<0.001
ABS	Scapula	0.086
	HEART	<0.001
	LUNG	<0.001
	LIVER	<0.001
	Right Rib	<0.001
	Vertebra	<0.001
PVA	Scapula	0.917
	HEART	0.004
	LUNG	<0.001
	LIVER	<0.001
	Right Rib	<0.001
	Vertebra	<0.001
ABSpremium	Scapula	0.955
	HEART	0.005
	LUNG	<0.001

*p-value of < 0.05 was considered as statistically significant

The radiographic imaging of the chest is one of the most common examinations performed in medical facilities. The efficiency in delivering important clinical insights quickly and affordably at low radiation doses is well-known [25]. In terms of optimizing imaging techniques for chest radiography, anthropomorphic phantoms play a significant role in evaluating imaging quality, as they are designed to mimic human tissue during X-ray examinations [26–28]. Furthermore, imaging professionals have also utilized anthropomorphic phantoms for educational and training purposes, such as learning how to operate imaging devices[29]. This study used a standard chest anthropomorphic phantom that presents the same x-ray attenuation of the adult male human.

The advancement in 3D printing techniques, accompanied by the vast array of materials available for printing customized objects for specific purposes, has stimulated investigation into 3D printing filaments that can be used to create educational models [30]. The representation of human tissues in anthropomorphic phantoms, through the deposition of melted plastic, is intrinsically related to the X-ray absorption properties of the tissues, and it is essential for the development of increasingly realistic models. In this study, we investigated imaging parameters in radiological imaging. We compared the values obtained from plastic materials made with 3D printing with those from structures of an anthropomorphic chest phantom, used as a reference for plastic materials comparison.

Significant differences were found when comparing the signal-to-noise ratio for plastic materials and chest structures. Similar results were found for the contrast-to-noise ratio. The differences were noted for both plastic materials, Tungsten and Bismuth, that demonstrated statistically significant values of signal-to-noise ratio compared to the lung ($p < 0.0001$) and right rib ($p < 0.0001$). The signal-to-noise ratio is related to the square root of the contrast in the number of photons transmitted [31]. This result shows that the Tungsten and Bismuth filaments may potentially represent the signal-to-noise ratio for intermediary and high-density structures. Scapula was the only anatomical structure with no statistically

significant difference of the contrast-to-noise ratio for SILK ($p \geq 0.074$), ABS ($p \geq 0.086$), PVA ($p \geq 0.917$) and ABSpremium ($p \geq 0.955$).

The tungsten and bismuth cubes showed higher contrast-to-noise ratio values compared to the other plastic materials. Regarding chest imaging, the lung, right rib, and vertebra showed higher contrast-to-noise ratio values compared to the heart, liver, and scapula. The cubes made of Tungsten and Bismuth showed lower mean pixel values. It represents the high attenuation feature of these plastic materials. Meanwhile, the lungs and ribs have higher mean pixel values for anthropomorphic phantom.

The plastic materials ABS, PLA, TPU, and PVA have been validated as suitable for radiotherapy and high energy photons, serving as tissue-equivalent materials for printing. They are used to improve the uniformity of dose distribution over irregular surfaces [32]. However, for the diagnostic energy range of photons used in this study, PLA and TPU showed lower contrast-to-noise ratio values and were discrepant from the anthropomorphic structures. Zhang et al. [28] created a 3D-printed thoracic phantom for radiotherapy quality control and dose verification using ABS to fat and chest wall. In addition, the radiation equivalent material of ribs, sternum and scapula were made with modified resin polymer material. For computed tomography, filament infused with bismuth and diluted with ABS has shown the potential to adjust the filament's radiodensity to represent bones [33].

The development of an anthropomorphic chest phantom has been described in the literature has been applicable in radiotherapy purposes [34–37]. Jung et al [34] used PLA to represent lung tissue, while Kairn et al.[38] found that the lung tissue can be represented depending on ABS infill percentage. However, neither study included the anatomy of vertebrae and ribs. Nylon has been reported as a material for lung representation as well [36,37]. Pallota et al.[35] printed the ribs using ABS+, a mixture of calcium sulfate dehydrate, and the authors found that radiopaque filaments (Bismuth and Tungsten) showed no differences in terms of the signal-to-noise ratio for the vertebra and rib. Although most of the newly developed 3D-printed anthropomorphic phantoms have been made for

radiotherapy and computed tomography purposes, the imaging properties of the plastic materials presented in this paper may be helpful for universities and industries to create their phantoms according to different needs and applications. Our work presented insights that can improve the affordability of diagnostic radiology phantoms by comparing these materials with typical chest phantom constructions. 3D printing technologies such as Stereolithography (SLA), Digital Light Processing (DLP), and polyjet have great potential for phantom development. However, regarding the development of 3D-printed thoracic phantoms, FFF is still the most widely applied printing method reported in the literature[22].

Regarding the widespread use of the FFF technique, the cost-effective and accessibility for producing 3D-printed phantoms are considered the most important reasons for the widely use of the FFF. the Tungsten and Bismuth filaments present the potential to simulate high-density structures like bones because of their high signal-to-noise ratio and contrast-to-noise ratio values. In addition, materials like SILK and PVA demonstrated the closest contrast-to-noise ratio match to the scapula among soft tissue analogues.

4. CONCLUSIONS

The study of potential radiological 3D printing materials for diagnostic radiology phantom development revealed important imaging characteristics for the plastic materials using the Fused Filament Fabrication technique. The radiopaque filaments (Bismuth and Tungsten) represented the signal-to-noise ratio of the vertebra and rib. The scapula was the only anatomical structure with no statistically significant difference in the contrast-to-noise ratio for SILK, ABS, PVA, and ABSpremium.

Research on 3D printing filaments represents a significant impact within diagnostic radiology and low-energy radiation therapy. Subsequent studies can investigate the performance of these materials in CT scanners and mammography units to evaluate the effect of the various filtration techniques and the performance of these materials as a bolus in radiotherapy.

ACKNOWLEDGMENT

The authors would like to thank the Federal Institute of Bahia, Brazil, GTecRAD (Grupo de Pesquisa em Tecnologia em Radiologia), LABIMM and LABmais3D/IFSC, for their help inconducting this study;

CONFLICT OF INTEREST

All authors declare that they have no conflicts of interest.

REFERENCES

[1] CRAMER, J.; QUIGLEY, E.; HUTCHINS, T.; , SHAH, L. Educational Material for 3D Visualization of Spine Procedures: Methods for Creation and Dissemination **J. Digit. Imaging,** v.30, n.3,p.296-300, 2017.

[2] KAMOMAE. T.;, SHIMIZU, H.; NAKAYA, T.; OKUDAIRA,K.;AOYAMA, T.; OGUCHI, H.; KOMORI, M.; KAWAMURA, M.; OHTAKARA,K.; MONZEN, H.; ITOH, Y.; NAGANAWA,S.; Three-dimensional printer-generated patient-specific phantom for artificial in vivo dosimetry in radiotherapy quality assurance **Phys. Medica**, v. 44 , p. 205-211, 2017

[3] SCULPTEO. The State of 3D Printing Report 2018 Disponível em: https://www.sculpteo.com/en/ebooks/state-of-3d-printing-report-2018/. Acesso em: 27 ago. 2024

[4] SHIN, J.; SANDHU, R.. S.; SHIH, G.; Imaging Properties of 3D Printed Materials: Multi-Energy CT of Filament Polymers **J. Digit. Imaging**, v.30,n.5, p.572–5, 2017

[5] YANG, L.; GROTTKAU, B.; HE, Z.; YE, C. Three dimensional printing technology and materials for treatment of elbow fractures **Int. Orthop**., v.41,p. 2381–2387, 2017.

[6] FAROOQI, K. M.; SAEED, O.; ZAIDI, A.; SANZ, J.; NIELSEN, J. C.; HSU, D. T.; JORDE, U. P. 3D Printing to Guide Ventricular Assist Device Placement in Adults With Congenital Heart Disease and Heart Failure. **JACC Hear**. v.4,n.4, p.301-11, 2016

[7] SAVI, M.; ANDRADE, M. A. B.; POTIENS, M. P. A. Commercial filament testing for use in 3D printed phantoms, **Radiat. Phys. Chem.,** v. 174, p, 108906, 2020

[8] SAVI, M.; ANDRADE, M. A. B.; VILLANI, D., JUNIOR, O. R.; POTIENS, M. D.A. P. A. Development of radiopaque FFF filaments for bone and teeth representation in 3D printed radiological objects, **Brazilian J. Radiat. Sci**. v.10,n.1,p.01-22,2022.

[9] KAPETANAKIS, I.; FOUNTOS, G.; MICHAIL, C.; VALAIS, I.; KALYVAS, N.; 3D printing X-Ray Quality Control Phantoms. A Low Contrast Paradigm, **Journal of Physics: Conference Series,**v.931,p. 012026,2017

[10] OLIVEIRA, M.; BARROS, J.C.; UBEDA, C. Development of a 3D printed quality control tool for evaluation of x-ray beam alignment and collimation, **Phys. Medica**, v. 65, p.29-32, 2019.

[11] PAXTON. N.; SMOLAN, W.; BÖCK, T.; MELCHELS, F.; GROLL, J.; JUNGST, T.; Proposal to assess printability of bioinks for extrusion-based bioprinting and evaluation of rheological properties governing bioprintability **Biofabrication** v.9,n.4,p.044107, 2017

[12] OGDEN,K. M.; MORABITO, K. E.; DEPEW, P. K.; 3D printed testing aids for radiographic quality control **J. Appl. Clin. Med. Phys**. v.20,n.5,p. 127–34,2019

[13] NOONOO. J, B.; SOSU, E.; HASFORD, F.; Three-dimensional image quality test phantom for planar X-ray imaging. **S. Afr. J. Sci**.v.119,n.7/8, p.1-7,2023

[14] MADAMESILA, J.; MCGEACHY, P.; VILLARREAL, B.J. E.; KHAN, R. Characterizing 3D printing in the fabrication of variable density phantoms for quality assurance of radiotherapy, **Phys. Medica**, v.32,n1,p.242-247, 2016

[15] GROENEWALD, A.; GROENEWALD, W. A. Development of a universal medical X-ray imaging phantom prototype **J. Appl. Clin. Med. Phys.** v.17,n.6,p356-365,2016.

[16] SCHOPPHOVEN, S.; CAVAEL, P.; BOCK, K.; FIEBICH, M.; MÄDER, U. Breast phantoms for 2D digital mammography with realistic anatomical structures and attenuation characteristics based on clinical images using 3D printing **Phys. Med. Biol**.v. 64,n.21,p.215005,2019

[17] HE, Y.; LIU, Y.; DYER, B. A.; BOONE, J. M.; LIU, S.; CHEN, T.; ZHENG, F.; ZHU, Y.; SUN, Y.; RONG, Y.; QIU, J.;3D-printed breast phantom for multi-purpose and multi-modality imaging **Quant. Imaging Med. Surg**. v.9,n.1,p.63-74 ,634–74,2019.

[18] OLIVEIRA, M.; SAVI, M.; ANDRADE, M.; VILLANI, D.; POTIENS, M. P. A.; STUANI, H; UBEDA, C.; MDLETSHE, S.; Attenuation properties of common 3D printed FFF plastics for mammographic applications **Brazilian J. Radiat. Sci**.,v. 10.n.1,p.01-17,2022

[19] LEE, M. Y.; HAN, B.; JENKINS, C.; XING, L.; SUH, T. S.; A depth-sensing technique on 3D-printed compensator for total body irradiation patient measurement and treatment planning **Med. Phys.** v.43,n.11,p.6137,2016

[20] JAVAN, R.; BANSAL, M.; TANGESTANIPOOR, A. A prototype hybrid gypsum-based 3-dimensional printed training model for computed tomography-guided spinal pain management **J. Comput. Assist. Tomogr**.v.40,n.4,p.626-631,2016

[21] KIM, M. J.; LEE, S. R.; LEE, M. Y.; SOHN, J. W.; YUN, H. G.; CHOI, J. Y.; JEON, S. W.; SUH, T. S. Characterization of 3D printing techniques: Toward patient specific quality assurance spine-shaped phantom for stereotactic body radiation therapy **PLoS One**, v.12,n.5,p.e0176227,2017

[22] SILBERSTEIN, J. ; SUN, Z. Advances and Applications of Three-Dimensional-Printed Patient-Specific Chest Phantoms in Radiology: A Systematic Review **Appl. Sci.** v.. 14, p. 5467 14 5467, 2024

[23] Rasband W. ImageJ. Bethesda, Maryland, USA: U.S. National Institutes of Health; 1997e2012. Disponivél em:: http://imagej.nih.gov/ij/.

[24] HUDA, W.; ABRAHAMS, R. B. Radiographic techniques, contrast, and noise in x-ray imaging. **Am. J. Roentgenol.** v.204,n.2,p. W126–31,2015

[25] BRODER, J. Imaging the Chest: The Chest Radiograph. **In Diagnostic Imaging for the Emergency Physician**, Expert Consult - Online and Print, p.185–296, 2011.

[26] DUKOV, N.; BLIZNAKOVA, K.; OKKALIDIS, N.; TENEVA, T.; ENCHEVA, E.; BLIZNAKOV, Z.; Thermoplastic 3D printing technology using a single filament for producing realistic patient-derived breast models, **Phys. Med. Biol.** v.67,n.4,p.045008,2022

[27] GEAR, J. I.; LONG, C.; RUSHFORTH, D.; CHITTENDEN, S. J.; CUMMINGS, C.; FLUX, G. D. Development of patient-specific molecular imaging phantoms using a 3D printer **Med. Phys.** v. 41,n.8,p.082502,2014.

[28] ZHANG, F.; ZHANG, H.; ZHAO, H.; HE, Z.; SHI, .; HE, Y.; JU, N.;RONG, Y.; QIU, J. Design and fabrication of a personalized anthropomorphic phantom using 3D

printing and tissue equivalent materials, **Quant. Imaging Med. Surg.** v.9,n.1,p.94-100,2019

[29] ANWARI, V.; LAI, A.; URSANI, A.; REGO, K.; KARASFI, B.; SAJJA, S.; PAUL, N. 3D printed CT-based abdominal structure mannequin for enabling research. **3D Print. Med.**v.6,n.1,p.1-12 ,2020

[30] PULLEN, M. W.; POOLEY, R. A.; KOFLER, J. M.;VALERO-MORENO, F.; RAMOS-FRESNEDO, A.; DOMINGO, R. A.; PEREZ-VEGA, C.; FOX, W. C.; SANDHU, S. J. S. QUINONES-HINOJOSA, A.; BUCHANAN, I. A. A radiographic analysis of common 3D print materials and assessment of their fidelity within vertebral models **Ann. 3D Print. Med**.v.8,p.1-7,2022

[31] HUDA, W.; BRAD, A.R. X-ray-based medical imaging and resolution **Am. J. Roentgenol**. v.204,n.4,p. W393–397,2015

[32] ZHAO, Y.; MORAN, K.; YEWONDWOSSEN, M.; ALLAN, J. CLARKE, S.; RAJARAMAN, M.; WILKE, D.; JOSEPH, P.; ROBAR, J. L. Clinical applications of 3-dimensional printing in radiation therapy **Med. Dosim**. v.42,n.2,p. 150–155,2017

[33] CEH, J.; YOUD, T.; MASTROVICH, Z.; PETERSON, C.; KHAN, S.; SASSER, T. A.; SANDER, I. M.; DONEY, J.; TURNER, C.; LEEVY, W. M. Bismuth Infusion of ABS Enables Additive Manufacturing of Complex Radiological Phantoms and Shielding Equipment. **Sensors (Basel)**.v. 17,n.3,p.459,2017

[34] JUNG, J.; SONG, S. Y.; YOON, S. M.; KWAK, J.; YOON, K.; CHOI, W.; JEONG, S. Y.; CHOI, E. K.; CHO, B. Verification of accuracy of CyberKnife tumor-tracking radiation therapy using patient-specific lung phantoms **Int. J. Radiat. Oncol. Biol. Phys.**v. 92,n.4,p.745-753,2015

[35] PALLOTTA, S.; CALUSI, S.; FOGGI, L.; LISCI, R.; MASI, L.; MARRAZZO, L. TALAMONTI, C.; LIVI, L.; SIMONTACCHI, G.ADAM: A breathing phantom for lung SBRT quality assurance **Phys. Medica,**v.49,p.147-155,2018

[36] LARSSON, J.; LIAO, P.; LUNDIN, P.; KRITE, S.E., SWARTLING, J.; LEWANDER, X. M.; BOOD, J.; ANDERSSON-ENGELS, S. Development of a 3-dimensional tissue lung phantom of a preterm infant for optical measurements of oxygen—Laser-detector position considerations, **J. Biophotonics**,v.11,n.3,p.1-8,2017

[37] HAZELAAR, C.; VAN EIJNATTEN. M.; DAHELE, M.; WOLFF, J.; FOROUZANFAR, T.; SLOTMAN, B.; VERBAKEL, W. F. A. R. Using 3D printing techniques to create an anthropomorphic thorax phantom for medical imaging purposes **Med. Phys.** v.45,n.1,p.92-100,2018.

[38] KAIRN, T.; CROWE, S. B.; MARKWELL, T. Use of 3D printed materials as tissue-equivalent phantoms In: Jaffray, D. (eds) World Congress on Medical Physics and Biomedical Engineering, Toronto, Canada. **IFMBE Proceedings,**v.51,p.728-729,2015

5. LICENSE